Implementation of Numerical Models to Evaluate Intrinsic Residual Stresses in 3D Woven Composites by Blind Hole Drilling Tests

KOSTIANTYN VASYLEVSKYI, IGOR TSUKROV,
HILARY BUNTROCK, TODD GROSS and BORYS DRACH

ABSTRACT

3D woven carbon/epoxy composites are often produced using resin transfer molding technique which includes epoxy curing at elevated temperatures. The process may lead to accumulation of the intrinsic residual stresses during cooling of the material caused by the mismatch between carbon and epoxy coefficients of thermal expansion.

This paper deals with implementation of mesoscale finite element models to evaluate intrinsic residual stresses in 3D woven composites. The stresses are determined by correlation of the surface displacements observed after drilling 1-mm diameter blind holes with the corresponding predictions of the models.

We investigated how a numerical representation of the composite plate surface affects the correlation between the experimental measurements and numerical predictions and how it influences the evaluation of the process-induced residual stresses. It has been shown for ply-to-ply woven composites with different pick spacing that the absence of the resin layer leads to more accurate interpretation of the experimental measurements. The prediction of the average residual stress in the matrix phase of the composite was found to be sensitive to the surface representation accuracy, however, the residual stress magnitude and distribution was not affected fundamentally.

INTRODUCTION

The hole drilling experimental technique to measure residual stresses in homogeneous materials is well developed and has been used for several decades [1]. The technique involves drilling a hole in the material to release the residual stress,

Kostiantyn Vasylevskyi, Mechanical Eng., Univ. of New Hampshire, Durham, NH
Igor Tsukrov, Mechanical Eng., Univ. of New Hampshire, Durham, NH
Hilary Buntrock, Mechanical Eng., Univ. of New Hampshire, Durham, NH
Todd Gross, Mechanical Eng., Univ. of New Hampshire, Durham, NH
Borys Drach, Mechanical & Aerospace Eng., New Mexico State Univ., Las Cruces, NM

measuring the surface deformation around the hole caused by the drilling and using the measured deformation to quantify the residual stress. The method was originally proposed for isotropic materials but later expended to orthotropic materials as in [2]. Initially the change in strain at a fixed radius from drilling a hole was measured with strain gauge rosettes. However, the use of the gauges imposes certain limitations on a material specimen's geometry and test environmental conditions, requires extreme accuracy of drilling process and provides values of strain in a limited number of points.

Optical methods such as moiré interferometry [3], holographic interferometry [4], digital image correlation (DIC) [5] and speckle pattern interferometry [6] estimate the residual stress from measurements of the full surface displacement field resulting from hole drilling. The calculation of residual stress in the material can be performed analytically if the material is linear and homogenous in the case of a simplified stress-state, the interpretation of the displacement data becomes more challenging for more complicated spatial distributions of residual stresses and in the case of inhomogeneous materials.

Processing-induced residual stresses in 3D woven carbon/epoxy composite materials often accumulate during the material post-manufacturing cooldown due to the mismatch between coefficient of thermal expansion (CTE) of carbon-fiber preform and epoxy resin matrix. It has been shown that the magnitude of these stresses in the composite can be large enough to cause microcracking in the material, see for example [7]. Thus, it becomes crucial to determine the spatial distribution of the residual stress. We have used electronic speckle pattern interferometry (ESPI) to measure in-plane displacements caused by the release of residual stress during blind hole drilling in 3D woven composites [8]. The experimental measurements were correlated with meso-scale finite element (FE) models [9] to predict spatial distribution of the residual stress [10].

This paper investigates the influence of the local reinforcement morphology and weaving imperfections on the accuracy of the hole drilling simulation results. We also determine how FE predictions of the displacements due to hole drilling are influenced by the composite plates surface epoxy resin layer (RL).

EXPERIMENTAL METHODS

The composite plates were manufactured exclusively for this research by Albany Engineered Composites using Hexcel RTM6 resin and Hexcel 12K IM7 PAN-based carbon fibers. Two ply-to-ply reinforcement architectures having different number of picks-per-inch (PPI) and labeled as 12×10 PPI and 12×12 PPI were considered, see TABLE I. (Table 1 also provides volume fractions (V_f) of tows in warp and weft directions which are discussed later in the text). The specimens were at least several unit cells of size (UC) (the smallest periodic repeatable portion of the material) to avoid any possible boundary effects. The specimens were first painted in white and then 5 -10 μm sized speckles were applied using an air brush. Then, the specimens were coated with a clear matte spray paint to protect the surface from defects during the hole drilling and handling. To ensure the successful correlation of the interferometric measurements, the specimens were glued to a Thor Labs kinematic mount that allowed precise repositioning after hole drilling.

TABLE I. Ply-to-ply reinforcement parameters and composite phases volume fractions

	V_f, %					
	Nominal geometry		FEA			
Picks/Inch	Warp	Weft	Warp, RL	Weft, RL	Warp, no RL	Weft, no RL
12×10	36.16%	32.58%	37.57%	35.08%	40.83%	37.47%
12×12	37.41%	39.10%	34.57%	39.30%	37.13%	41.29%

The blind holes were 1 mm diameter and 0.5 mm depth. The depth is similar to the thickness of the tows and the diameter is roughly half the width of the tow. A UKAM diamond coring tool was used for drilling. The specimen was cooled down during the drilling process using deionized water flow which also served to remove debris. The in-plane displacements around the hole were measured using a custom-built electronic speckle pattern interferometry system with a linearly polarized, 50 mW Melles Griot HeNe laser. The accuracy of the measured displacements was estimated to be around 9 nm from the noise amplitude from repeated measurements on specimens that were not moved. A more detailed description of the experimental set-up and procedure can be found in [8].

NUMERICAL SIMULATIONS

Two 3D woven ply-to-ply composite material unit cells were simulated. The numerical as-woven representation of the material reinforcement fabric was prepared using Digital Fabric Mechanics Analyzer (DFMA) [11]. The finite element mesh of the reinforcement and the corresponding epoxy resin matrix phase were created using MSC.Marc Mentat (https://www.mscsoftware.com/product/marc). Figure 1 shows the FE mesh of the 12×10 PPI ply-to-ply reinforced composite.

The epoxy resin matrix phase was assumed to be temperature-dependent isotropic elastic material with constant Poisson's ratio and temperature dependent Young's modulus and CTE. The reinforcement phase of the composite was treated as a transversely isotropic unidirectional composite and its effective mechanical properties were obtained using micromechanical modeling. The elastic properties of the reinforcement were assumed to be temperature independent due to a high volume fraction of carbon fibers (80%). (for a detailed description see [12])

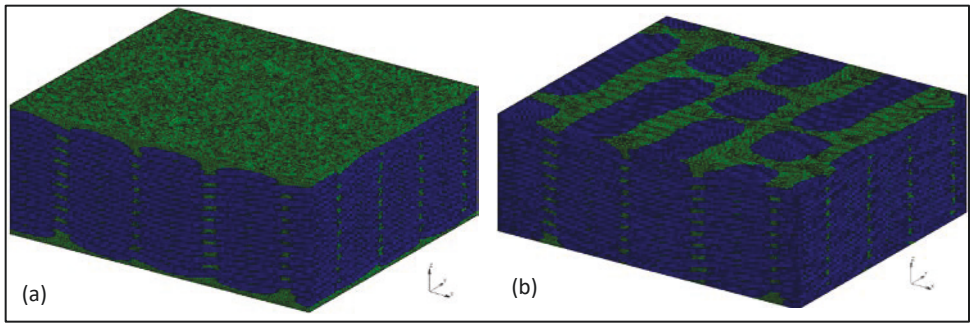

Figure 1. FE mesh of a ply-to-ply 12×10PPI composite (a) with and (b) without resin layer on top and bottom of the composite plate.

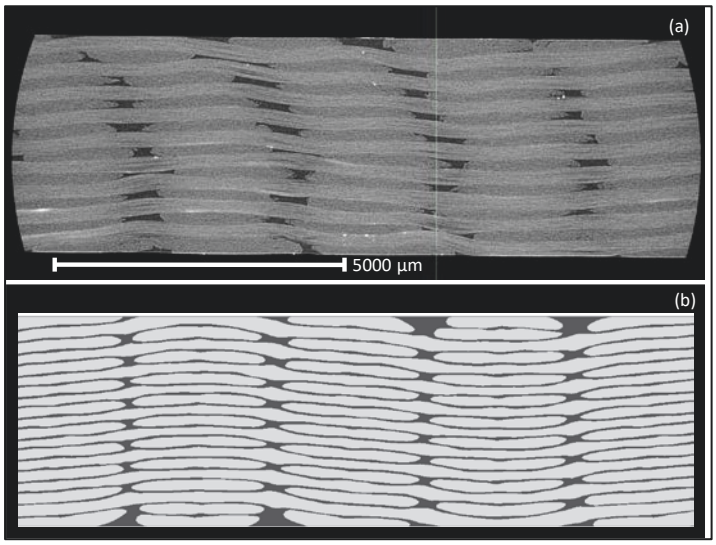

Figure 2. Cross-section view of the 12×10 PPI composite plate (a) obtained from µCT and (b) simulated using FEA without the epoxy layer over the tows. Note the weaving imperfection demonstrated by violation of vertical alignment of weft tow columns in µCT image.

Cooling After Curing and Drilling Simulation

The cooling after curing (from 165° C to 20° C) and hole drilling simulations were performed using MSC Marc Mentat software. The material was assumed to be fully cured and stress-free in the beginning of the cooling process. The temperature drop was simulated using thermal state variable of the finite element mesh. The drilling was simulated by the deactivation of finite elements in the location of the hole. The results are presented as color plots of displacement fields due to drilling and as graphs of the displacement along horizontal (warp) and vertical (weft) slice lines. As has been shown in [10], the hole location with respect to the reinforcement features significantly influences displacements around the hole, thus two precise hole locations were chosen for each reinforcement architecture. The simulations were performed for a single unit cell of the material with periodic boundary conditions allowing free shrinkage of the specimen during cooling.

Surface Resin Layer Simulation

Mesoscale FE models of 3D woven composites sometimes include a surface layer of

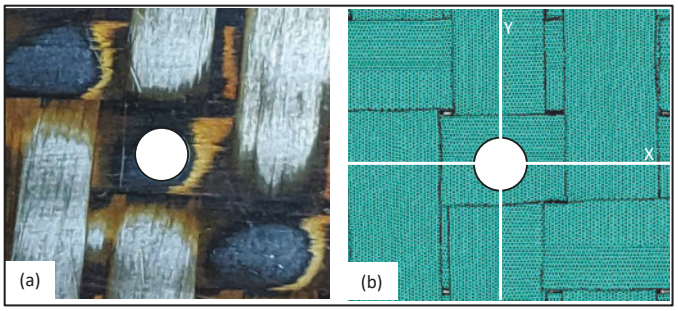

Figure 3. 12×10 PPI warp hole location (a) as in the experiment and (b) as in the model.

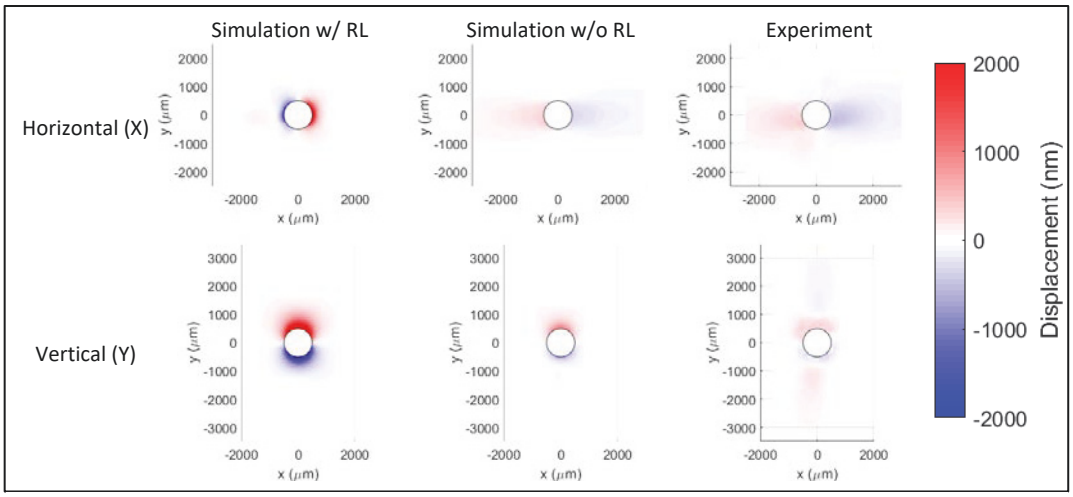

Figure 4. Displacement fields comparison for 12×10 PPI (hole cutting a top warp tow).

resin completely covering the reinforcement tows ([13] and [14]) and sometimes have the tows exposed on the surface ([15] and [16]). In most cases this thin layer of resin is not important for evaluation of the overall stiffness and strength of the material. However, its presence can be crucial for interpretation of the hole drilling experiments. In this paper, we investigate the importance of accurate representation of the surface topology for successful evaluation of residual stresses in composite specimens.

Figure 2 (a) shows a microtomography (μCT) image of 12×10 PPI composite plate obtained using a Zeiss Xradia 610 system with 5.99 μm resolution. It shows that there is no epoxy resin on the top and bottom surfaces in the region of the tows. We investigated how the presence or absence of the surface resin layer on top of the tow affects the correlation of the hole drilling numerical and experimental results and also how the resin layer influences the predicted intrinsic residual stresses in the material. Two sets of FE models, with and without resin layer on the tows, were created (Figure 1). The thickness of the layer on top of the tows in the modelled UCs varies from 50 – 110 μm for 12×10 PPI and 30 – 110 μm for 12×12 PPI. This corresponds to 1-2 finite elements.

Both 12×10 PPI and the 12×12 PPI reinforcement architectures were simulated

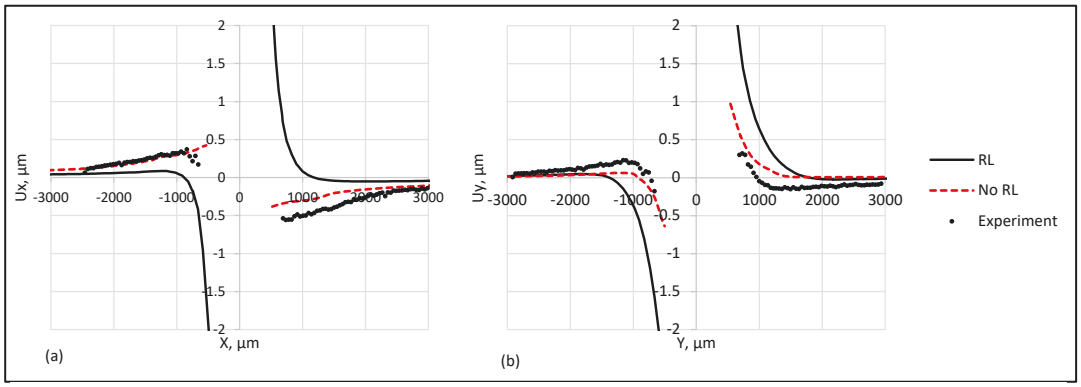

Figure 5. Slice plots for the warp hole (a) in parallel-to-the-tow and (b) transverse directions, for 12×10 PPI.

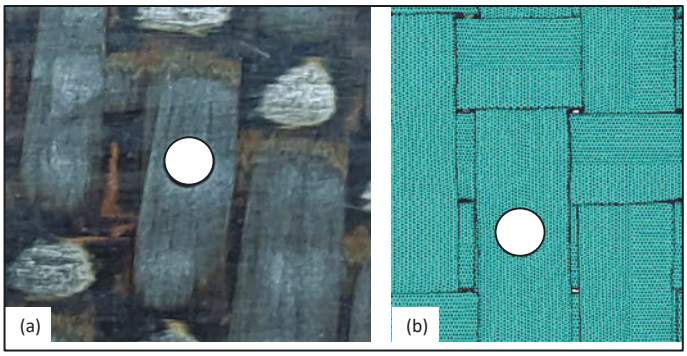

Figure 6. 12×10 PPI weft hole location (a) as in the experiment and (b) as in the model.

using quadratic tetrahedral elements. Initially, the models with the resin layer were created. Then, the resin on the top and bottom of the unit cell was manually removed, and the mesh was modified in a way that the surface layers of the preform are exposed (as it is seen in the μCT image) whereas the surface is kept flat.

The in-plane geometrical size of both unit cells remained the same (10.16mm × 8.47mm for 12×10 PPI and 8.47mm × 8.47mm for 12×12 PPI) and the thickness decreased by 9.1% and 7.4% for the 12×10 PPI and 12×12 PPI, respectively. This changed the volume fractions of the warp and weft yarns in the composite, as presented in TABLE I , however, the change was mostly due to a drop in the matrix phase volume. Note that the nominal geometry values presented in TABLE I are a preliminary estimate of the manufacturers based on the dry preform before resign impregnation.

RESULTS AND DISCUSSION

Figure 3 (a) shows a micrograph of the hole location in a warp tow in the 12×10 PPI ply-to-ply material and Figure 3 (b) shows the hole location in the FE

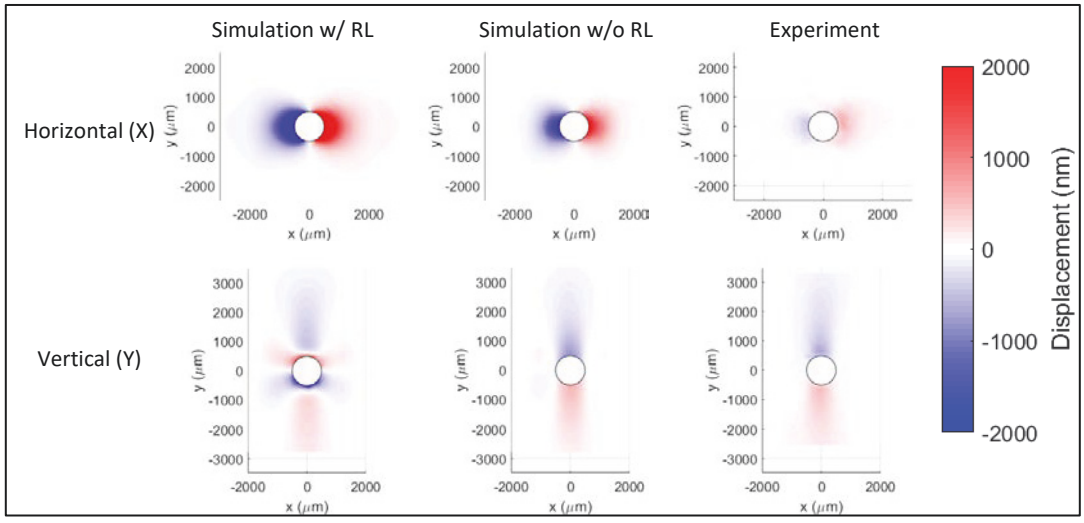

Figure 7. Displacement fields comparison for 12×10 PPI (hole cutting a top weft tow).

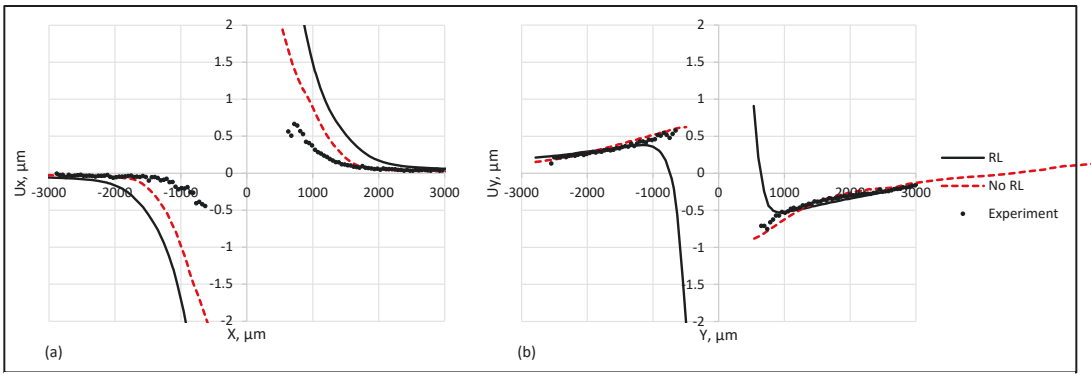

Figure 8. Slice plots for the weft hole in (a) transverse and (b) parallel-to-the-tow and directions, for 12×10 PPI.

model. The displacements fields for this hole location are shown in Figure 4 for the model with and without resin layer as well as experimental measurements.

As seen in this figure, the model without the resin layer is a better qualitative and quantitative match to both the vertical and horizontal displacements. The model with the resin layer exhibits opening in both directions which is consistent with a biaxial tensile stress of the surface layer. At the same time, according to the model, the tows are in compression along the axis of the tow and in tension transverse to the tow axis. This suggests that in the absence of the surface layer the displacements should be toward the hole in the warp direction and away from the hole in the weft direction. Thus, the surface displacements are strongly affected by the behavior of the top layer. When the model has the resin layer on top of the tow, it predicts surface displacements consistent with a biaxial tensile stress. When the resin layer is absent, as in the second model, the displacements reflect the state of stress in the tow.

Figure 5 shows slice plots of the horizontal and vertical displacements along the X and Y slice lines (Figure 3 (b)). Both displacement components show better agreement with the experimental data for the models without resin layer. However, the prediction and measurements do not perfectly agree. The difference is greater for the transverse to the tow direction which may be attributed to weaving imperfections (Figure 2 (a)) or possible nonlinear effects in the resin matrix.

Figure 6 shows hole cutting a top weft tow in the 12×10 PPI architecture. The contour maps of the displacement fields are shown in the Figure 7. Analogously to

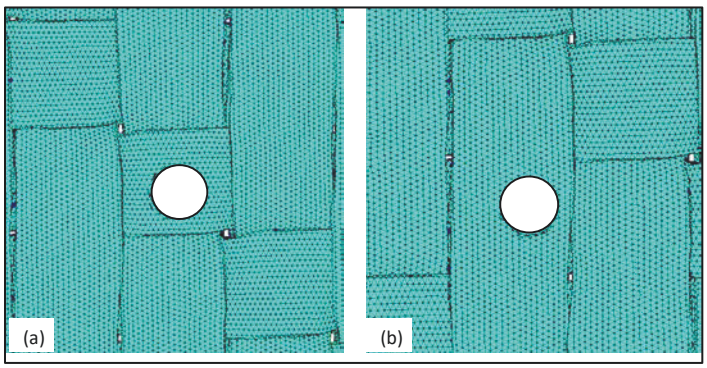

Figure 9. 12×12 PPI (a) warp hole location and (b) weft hole location.

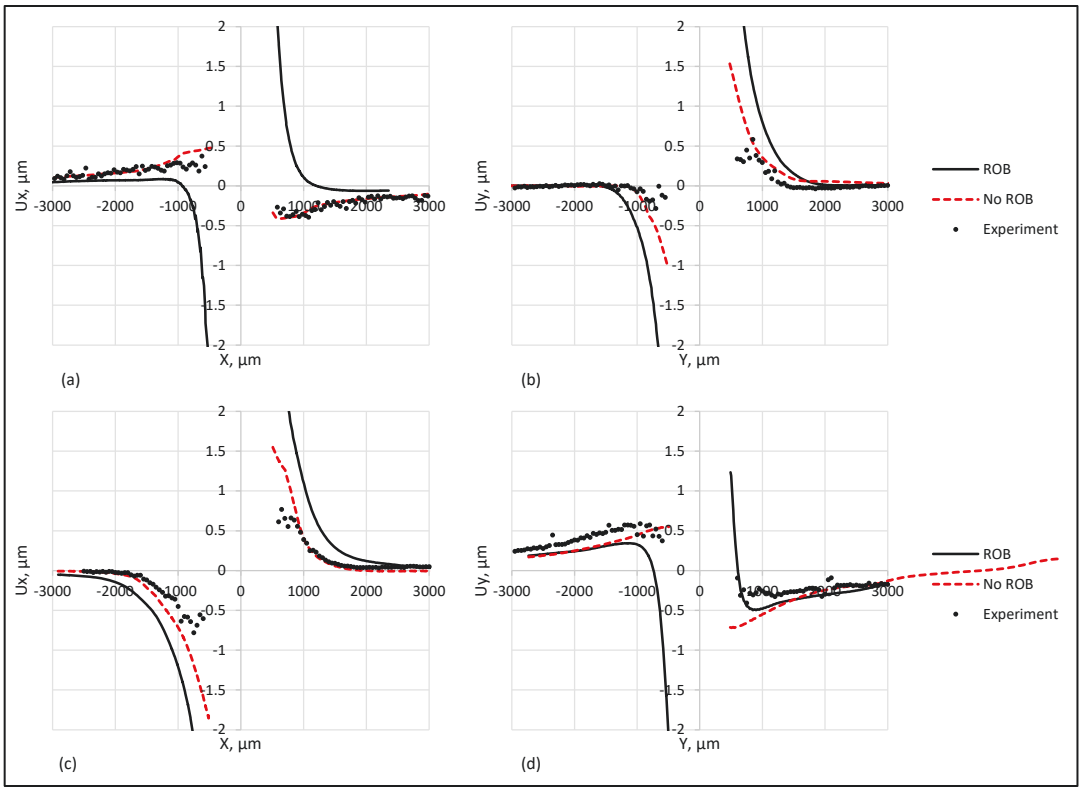

Figure 10. Slice plots for the (a) warp hole in parallel-to-the-tow and (b) transverse directions and (c) weft hole in transverse and (d) parallel-to-the-tow directions, 12×12 PPI.

the warp hole, the model with no resin layer shows better agreement with the experimental data. The magnitude of the displacements in the direction transverse to the tow reduced and the displacement field in the direction of the tow shows obvious closing of the hole as it is observed in the experimental data.

It is evident that removal of the resin layer results in improved prediction of the displacements especially close to the hole edge. Figure 8 shows slice displacements. The displacement in the direction transverse to the tow is overpredicted by both models, however model predictions with no layer shows better agreement with the measurements. Both model predictions agree with the experimental data except next to the hole edge for the model with the resin layer. This phenomenon can be explained by the thin layer of resin on top the tow in the model with the resin layer which is under tension. This causes the hole to "open" near the edge. The transverse direction displacements mismatch can potentially be related to the nonlinear behavior of the resin or due to the residual stresses relaxed in the material by the epoxy resin creep or cracking in either phase of the composite.

A 12×12 PPI ply-to-ply reinforced composite was also considered. Similar hole locations were chosen to investigate whether similar trends would be observed for the material with slightly different microstructure, namely different warp and weft columns spacing and hence different volume fractions of the reinforcement components. Figure 9 shows warp and weft hole locations in 12×12 PPI specimen models. The slice plots for these locations are shown in Figure 10.

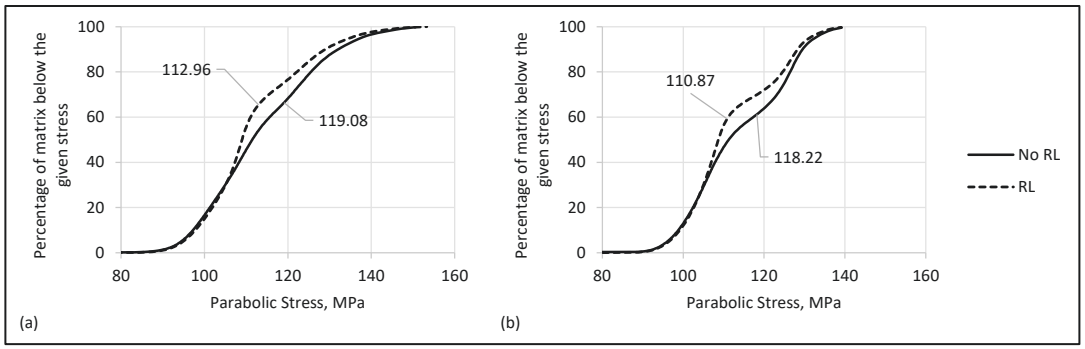

Figure 11. Distribution of parabolic equivalent stress within the matrix phase of the composite for (a) 12×10 PPI and (b) 12×12 PPI architectures.

In both cases model without the resin layer shows better agreement with the experimental data. Similar to the 12×10 PPI architecture, both models consistently overpredict the displacements transverse to the tow but the model without the resin is closer to the experimental results. The model without the layer exhibits good agreement for along-the-tow direction.

The model with the resin layer predicts a sign reversal near the edge of the hole for displacements parallel to the tow. This is not observed in the experimental data and is not predicted by the model without the resin layer. We attribute this to the prediction being strongly influenced by the top layer.

Surface Resin Layer Influence on Distribution of Residual Stress in the Material

We previously evaluated several failure criteria to determine which one most closely predicted the location of matrix microcracking observed in a 3D woven carbon/epoxy composite with an orthogonal reinforcement architecture [12]. In this work, we compared the cumulative distribution of the equivalent parabolic stress for the models with and without the resin layer, see Figure 11.

The curves show percentage of matrix phase volume under a certain value of the parabolic stress shown in the horizontal axis. It is seen that lower 40% and upper 10% of the resin volume are almost exactly the same for both cases, whereas middle range is different. The model without the resin layer predicts a slightly larger residual stress in the middle population of the volume. This can be attributed to the fact that the surface resin is under lower stress than that in the interior and removal of those elements results in an increase in the average stress.

SUMMARY AND CONCLUSIONS

We used numerical models to interpret hole drilling experiments on 3D ply-to-ply woven composites to evaluate their process-induced residual stresses. We compared numerical predictions for models with and without the surface resin layer. The removal of the resin layer from the UC surface led to a better agreement between simulated and experimentally measured displacement fields caused by the residual stress release. The measured displacements parallel to the tow matched particularly well with the models with no resin layer. The displacements transverse to the tow

were overpredicted by both numerical models with the model without the resin layer being much closer to the experimental measurements.

We performed quantitative comparison of the accumulated residual stress in the matrix phase of the composite as calculated by FE models with and without the resin layer. We found that since the removal of the surface layer increases, the percentage of the "interior" resin which is anticipated to be under higher residual stress, the average matrix stress is increased. However, the maximum stresses (presumably leading to failure) are unaffected.

ACKNOWLEDGEMENTS

This material is based upon work supported by the National Science Foundation, USA through grant CMMI-1662098.

REFERENCES

[1] Rendler, N. J., and Vigness, I., 1966, "Hole-Drilling Strain-Gage Method of Measuring Residual Stresses," Exp. Mech., **6**(12), pp. 577–586.

[2] Schajer, G. S., and Yang, L., 1994, "Residual-Stress Measurement in Orthotropic Materials Using the Hole-Drilling Method," Exp. Mech., **34**(4), pp. 324–333.

[3] Nicoletto, G., 1991, "Moiré Interferometry Determination of Residual Stresses in the Presence of Gradients," Exp. Mech., **31**(3), pp. 252–256.

[4] Makino, A., and Nelson, D., 1994, "Residual-Stress Determination by Single-Axis Holographic Interferometry and Hole Drilling-Part I: Theory," Exp. Mech., **34**(1), pp. 66–78.

[5] Lord, J. D., Penn, D., and Whitehead, P., 2008, "The Application of Digital Image Correlation for Measuring Residual Stress by Incremental Hole Drilling," Appl. Mech. Mater., **13–14**, pp. 65–73.

[6] Díaz, F. ., Kaufmann, G. ., and Galizzi, G. ., 2000, "Determination of Residual Stresses Using Hole Drilling and Digital Speckle Pattern Interferometry with Automated Data Analysis," Opt. Lasers Eng., **33**(1), pp. 39–48.

[7] Tsukrov, I., Bayraktar, H., Giovinazzo, M., Goering, J., Gross, T., Fruscello, M., and Martinsson, L., 2011, "Finite Element Modeling to Predict Cure-Induced Microcracking in Three-Dimensional Woven Composites," Int. J. Fract., **172**(2), pp. 209–216.

[8] Gross, T., Buntrock, H., Tsukrov, I., Drach, B., Vasylevskyi, K., and Chagnon, N., 2018, "Measurement of Intrinsic Residual Stresses in 3D Woven Composites Using Measurement of the Displacement Fields from Hole Drilling by Electronic Speckle Pattern Interferometry and Digital Image Correlation," *American Society for Composites 2018*.

[9] Drach, A., Drach, B., and Tsukrov, I., 2014, "Processing of Fiber Architecture Data for Finite Element Modeling of 3D Woven Composites," Adv. Eng. Softw., **72**, pp. 18–27.

[10] Vasylevskyi, K., Tsukrov, I., Drach, B., Buntrock, H., and Gross, T., 2020, "Identification of Process-Induced Residual Stresses in 3D Woven Carbon/Epoxy Composites by Combination of FEA and Blind Hole Drilling," Compos. Part A Appl. Sci. Manuf., **130**(July 2019), p. 105734.

[11] Miao, Y., Zhou, E., Wang, Y., and Cheeseman, B. A., 2008, "Mechanics of Textile Composites : Micro-Geometry," Compos. Sci. Technol., **68**(7–8), pp. 1671–1678.

[12] Drach, B., Tsukrov, I., Trofimov, A., Gross, T., and Drach, A., 2018, "Comparison of Stress-Based Failure Criteria for Prediction of Curing Induced Damage in 3D Woven Composites," Compos. Struct., **189**(January), pp. 366–377.

[13] Joglekar, S., and Pankow, M., 2017, "Modeling of 3D Woven Composites Using the Digital Element Approach for Accurate Prediction of Kinking under Compressive Loads," Compos. Struct., **160**, pp. 547–559.

[14] Patel, D. K., Waas, A. M., and Yen, C. F., 2018, "Direct Numerical Simulation of 3D Woven

Textile Composites Subjected to Tensile Loading: An Experimentally Validated Multiscale Approach," Compos. Part B Eng., **152**(February), pp. 102–115.
[15] Timoshchuk, N. V., Kasper, K. D., and Bayraktar, H. H., 2018, "Assessment of Process-Induced Microcracks in 3D Woven Composites Using Meso-Scale Model Simulations," IOP Conf. Ser. Mater. Sci. Eng., **406**(1).
[16] Yan, S., Zeng, X., and Long, A., 2019, "Meso-Scale Modelling of 3D Woven Composite T-Joints with Weave Variations," Compos. Sci. Technol., **171**(July 2018), pp. 171–179.